*Supporting Information*

# Delivery, Fate, and Mobility of Silver Nanoparticles in Citrus Trees

Yiming Su[1], Vanessa E. T. M. Ashworth[2], Nicholas K. Geitner[3], Mark R. Wiesner[3], Nichole Ginnan[4], Philippe Rolshausen[2], Caroline Roper[4], David Jassby[1,*]

[1]Department of Civil and Environmental Engineering, University of California, Los Angeles, *CA 90095*, United States
[2]Department of Botany and Plant Sciences, University of California, Riverside, *CA 92521*, United States
[3]Department of Civil and Environmental Engineering, Duke University, *NC 27708*, United States
[4]Department of Plant Pathology, University of California, Riverside, *CA 92521*, United States

*Email: jassby@ucla.edu.

## Derjaguin-Landau-Verwey-Overbeek (DLVO) model description

The Classical DLVO model includes Lifshitz-van der Waals ($U_{123}^{LW}$, attractive energy, Eq. S1) and electrostatic ($U_{123}^{EL}$, repulsive energy, Eq. S2) interactions between the NPs and the plant vessel surfaces (Eq. S3).[1]

$$U_{123}^{LW} = -\left(\frac{Ar}{6h}\right)\left(1+\frac{14h}{\lambda}\right)^{-1} \quad \text{(S1)}$$

$$U_{123}^{EL} = \pi\varepsilon_r\varepsilon_0 r\left(2\zeta_1\zeta_2 \ln\left(\frac{1+e^{-\kappa h}}{1-e^{-\kappa h}}\right) + \left(\zeta_1{}^2 + \zeta_2{}^2 +\right)\ln(1-e^{-2\kappa h})\right) \quad \text{(S2)}$$

$$U^{DLVO} = U_{123}^{LW} + U_{123}^{EL} \quad (S3)$$

where A is Hamaker constant (typically set as $10^{-20}$ J for NPs),[2,3] λ is the characteristic wavelength of the dielectric (typically taken as 100 nm), $\varepsilon_r$ is the dielectric constant, ranging between 20 to 40 for xylem/phloem sap (pure water is around 80),[4] $\varepsilon_0$ is the vacuum permittivity ($8.8541817\times10^{-12}$ F/m),[5] $r$ is the radius of NPs in synthetic sap derived from DLS intensity size (nm), $h$ is the separation distance between the NP and the lumen surface (nm), $\zeta_1$ and $\zeta_2$ are the surface charge of a NP and xylem/phloem (mV), respectively, and $\kappa$ is the Debye-Huckel parameter, which can be calculated *via*

Eq. S4,[1]

$$\kappa = \sqrt{\frac{e^2 \sum n_i z_i^2}{\varepsilon_r \varepsilon_0 k_B T}} \quad \text{(S4)}$$

Where $e$ is the electron charge, $k_B$ is Boltzmann's constant, $n_i$ is the number concentration of ion $i$, and $z_i$ is the valence of ion $i$. Based on previous studies,[6–9] the surface potential of xylem and phloem was set as -90 mV and -150 mV, respectively, and the Debye length for the phloem and xylem was determined to be 1.0 and 5.0, respectively.

**Polymer layer thickness estimation**

The polymer layer thickness of PVP was estimated using a simplified Ohshima's polymer coated (soft) particle model. PVP is an uncharged polymer with a frictional parameter ($0<\lambda<$N, with N a number, not $\infty$), both $\lambda d$ and $\kappa d$ >1 ($\kappa$ is Debye-Hückel parameter; $d$ is the layer thickness). In the synthetic sap, $\zeta$ (the zeta potential of the bare particles, -0.003 μm·s$^{-1}$·V$^{-1}$·m) is small, thus the relationship between mobility ($\mu$) and thickness ($d$) can be expressed by Eq. S5:

$$\mu = \frac{\varepsilon_r \varepsilon_0 \zeta}{\eta} \cdot \frac{1}{1-\left(\frac{\lambda}{\kappa}\right)^2} \cdot \left[\frac{1}{\cosh \lambda d} - (\lambda/\kappa) e^{-\kappa d}\left(\frac{\lambda}{\kappa} + \tanh \lambda d\right)\right] \quad \text{(S5)},$$

where $\varepsilon_r$ is the relative permittivity of water, $\varepsilon_0$ is the vacuum permittivity, $\eta$ is the viscosity of water, and $\zeta$ is the zeta potential of the bare particles. Due to the high ionic strength (467 mM) in synthetic sap, the calculated $d$ (derived from MATLAB, iterative least squares minimization) for PVP is about 4.4 nm. In addition, we calculated the thickness of the PVP under different ionic strengths (Figure S5), and found that the thickness can increase to 23.6 nm in a solution with 10 mM NaCl, which is in line with a previous study.[10]

In terms of GA-AgNP, since GA is negatively charged, Eq. S5 may not be appropriate (though the thickness of GA estimated by Eq. S5 is 4.8 nm in synthetic sap). Given that the molecule weight of GA is almost an order of magnitude higher than PVP, it is assumed that the molecular weight ($M_w$) dominates the change in polymer layer thickness according to the work of Baker *et al.*[11] In their study,[11] the polymer layer thickness is a linear function of $M_w^{0.65}$, and therefore the thickness of the GA layer is estimated to be 20.1 nm (based on the data calculated for PVP, $d$ = 4.4 nm, $M_w$ = 40000).

**Electrode conditioning for Zeta potential measurement**

(1) Wet a Kimwipe with MilliQ water. (2) Pass the wipe through the gap in the electrode assembly. (3) Pass it back and forth against each electrode to clean off any black tarnish present. (4) Rinse the electrodes thoroughly with deionized water. (5) Fill a plastic cuvette with approximately 1.5 mL of 1M NaCl and insert the electrode assembly into the cuvette. (6) With the ZetaPALS, set up and make a single measurement of 350 cycles. (7) Afterwards, thoroughly rinse the electrodes with de-ionized water.

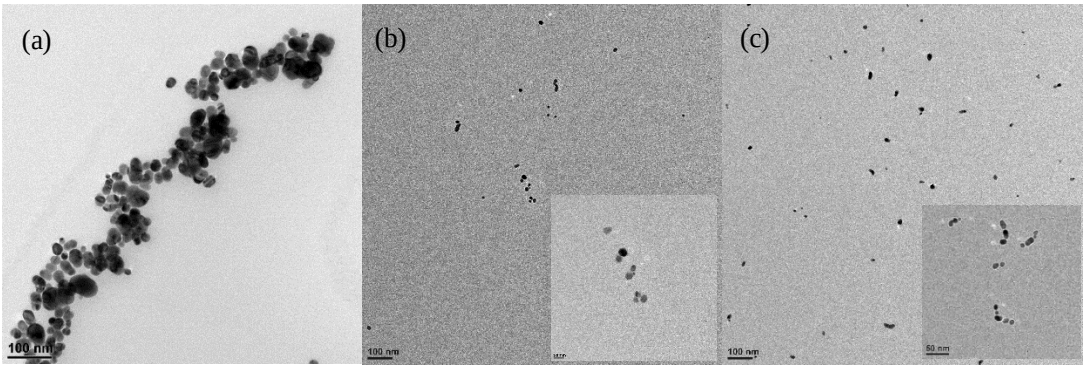


Figure S1. TEM images of AgNPs with different surface modifications: (a) Ct, (b) PVP, and (c) GA. (Scale bar in a, b, and c: 100 nm; scale bar in inserted figure, 50nm)

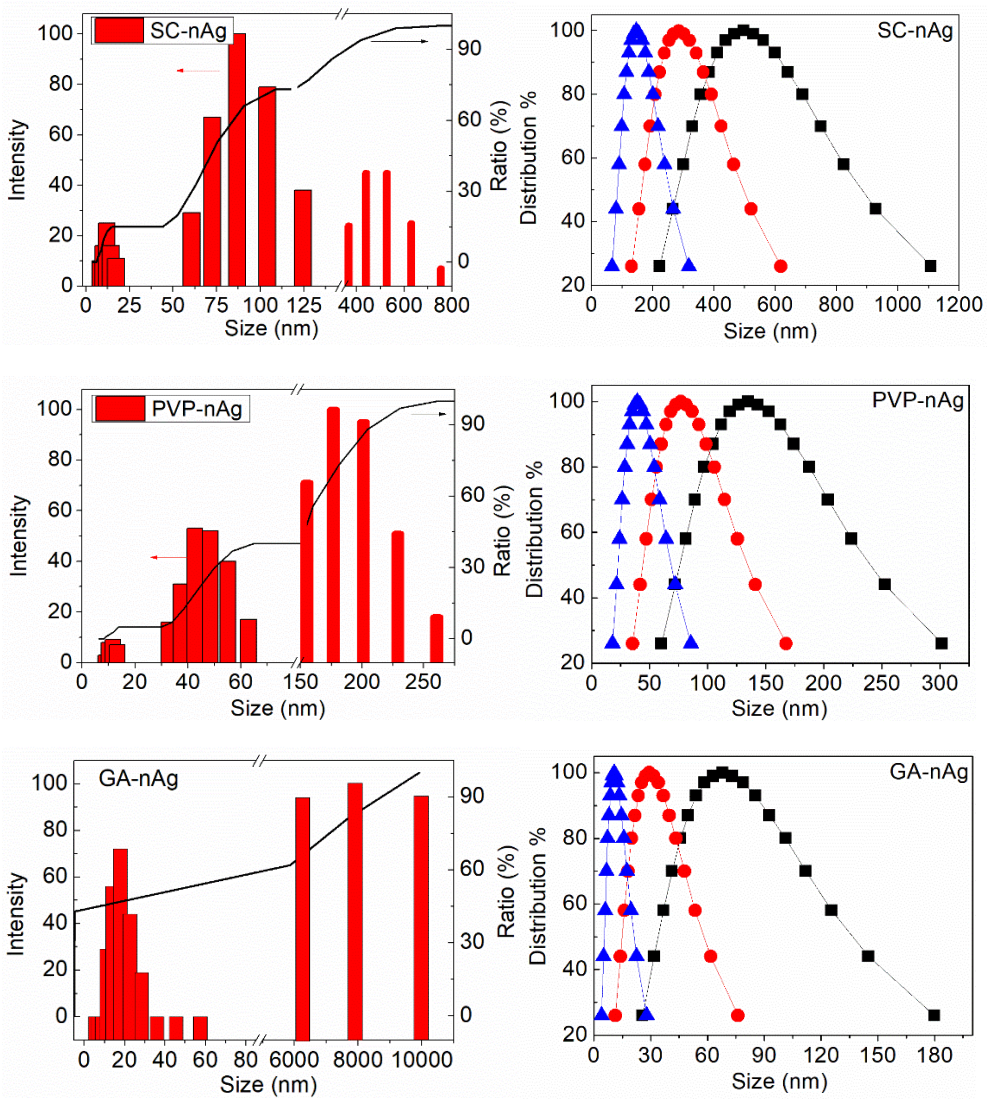


Figure S2. Size distribution of AgNP with different surface modification in DI water (a-c) and synthetic sap (d-f). ▲, number size; ●, volume size; ■, intensity size.

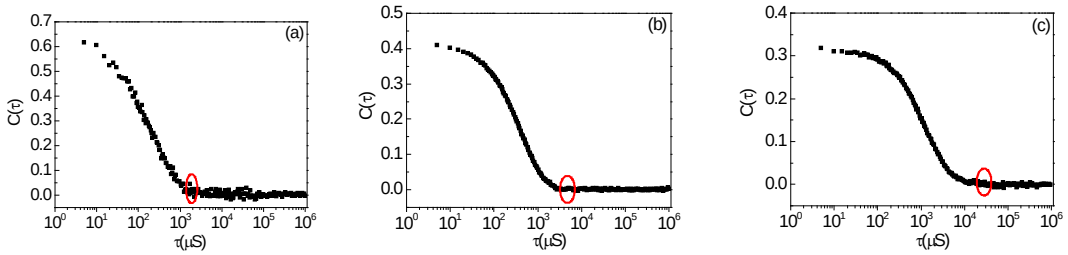


Figure S3. Correlograms for three DLS measurements in synthetic sap (10 ppm AgNP, pH=5.5): (a) GA-AgNP, (b) PVP-AgNP, and (c) Ct-AgNP. (dots in red oval are the signal of data collected by the instrument)

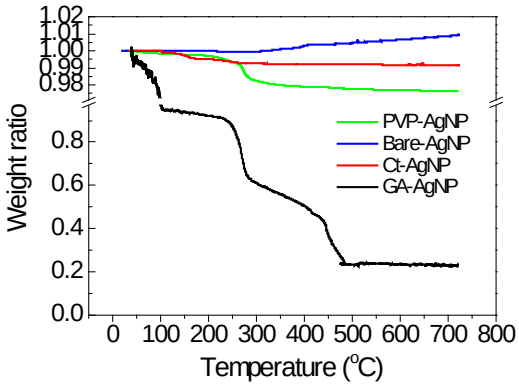


Figure S4. Weight change *vs.* temperature for each type of coated AgNP and bare AgNP. AgNPs were separated by ultracentrifugation (100000 rpm, 1 hour, Beckman Coulter, USA). All the AgNPs were dried in vacuum drier at 70 °C for 48 h before thermogravimetric analysis (TGA). The weight loss up to 150 °C (due to the loss of adsorbed water) of bare AgNP, Ct-AgNP and PVP-AgNP was negligible, but that of GA-AgNP was about 10%. The next weight loss occurred between 150 °C and 700 °C for Ct-AgNP, PVP-AgNP, and GA-AgNP were 0.9 ± 0.1%, 2.3 ± 0.3% and 67.3 ± 0.9%. In contrast, within the same temperature range, there was 1.0% weight increase for bare AgNP due to the oxidation of Ag(0). It is assumed that the weight changes for the coated AgNP are due to the Ag(0) oxidation and surface organic decomposition. Since TGA results for sodium citrate, GA, and PVP showed 45%, 100%, and 100% weight loss at 700 °C, respectively, citrate, PVP and GA on AgNP surface accounted for 1.9 ± 0.2%, 3.3 ± 0.3% and 68.3 ± 0.9% of the total weight, respectively. Furthermore, in theory, the surface area of 28 nm Ct-AgNP, 18 nm PVP-AgNP, and 10 nm GA-AgNP (diameter estimated from TEM analysis) are 20.4, 31.7 and 57.0 $m^2$, respectively. Therefore, the surface concentration of Ct, PVP and GA are 9.6 ± 0.5 × $10^{-4}$, 1.1 ± 0.1 × $10^{-3}$ and 5.3 ± 0.7 × $10^{-2}$ g/$m^2$, respectively.

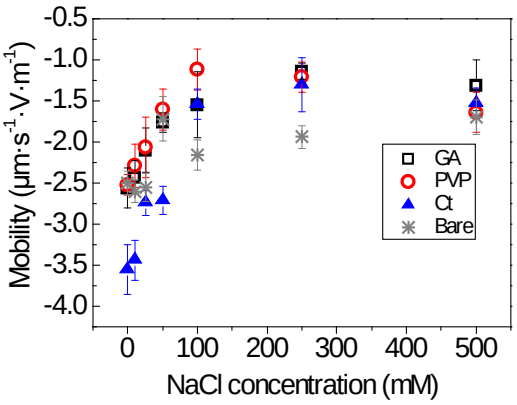


Figure S5. Electrophoretic mobility of bare and surface coated AgNPs. The electrophoretic mobility of bare AgNPs (*) as well Ct-AgNP (▲), PVP-AgNP (○), and GA-AgNP (□) (20 ppm, pH=5.5). In accordance with Ohshima's soft particle model, the PVP thickness out of PVP-AgNP in solution with 10, 25, 50, 100, 250, and 500 mM NaCl are 23.6, 15.2, 11.2, 7.6, 5.1, and 4.0 nm, respectively.

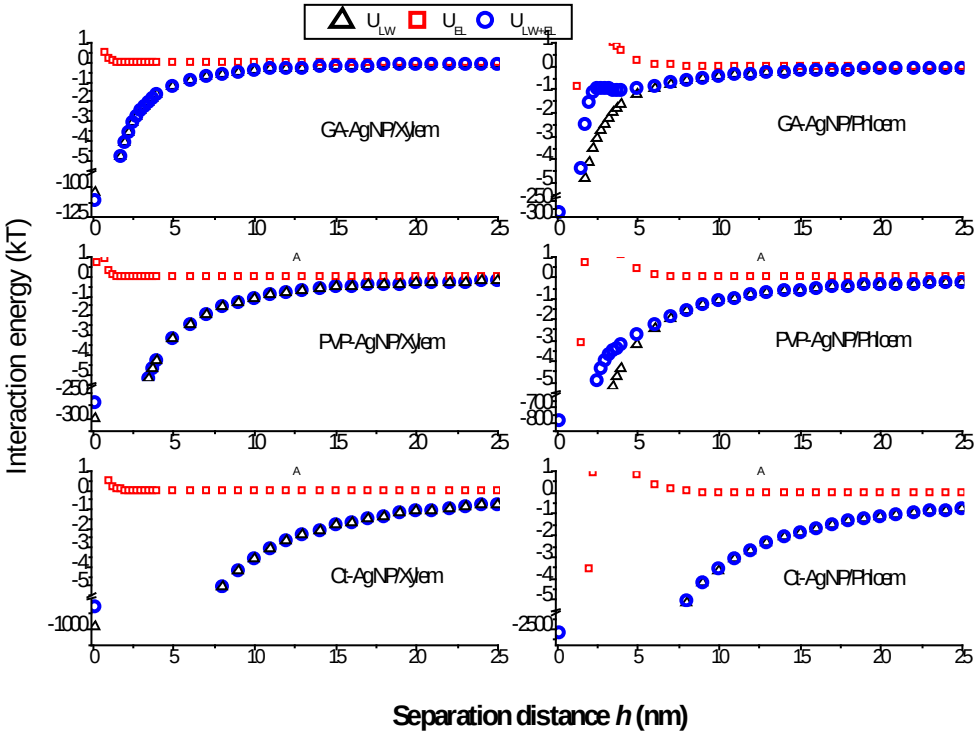


Figure S6. DLVO interaction energy profile between AgNP (PVP-AgNP, GA-AgNP and Ct-AgNP) and xylem/phloem surface: △, Lifshitz-van der Waals interaction; □, electrostatic interaction; ○, DLVO interaction

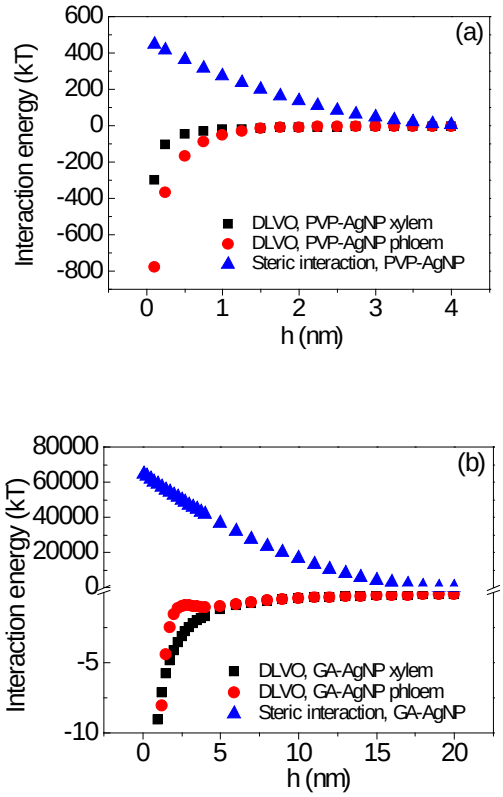


Figure S7. Classic DLVO and steric interaction energy between PVP-AgNP (a)/GA-AgNP (b) and xylem/phloem surface

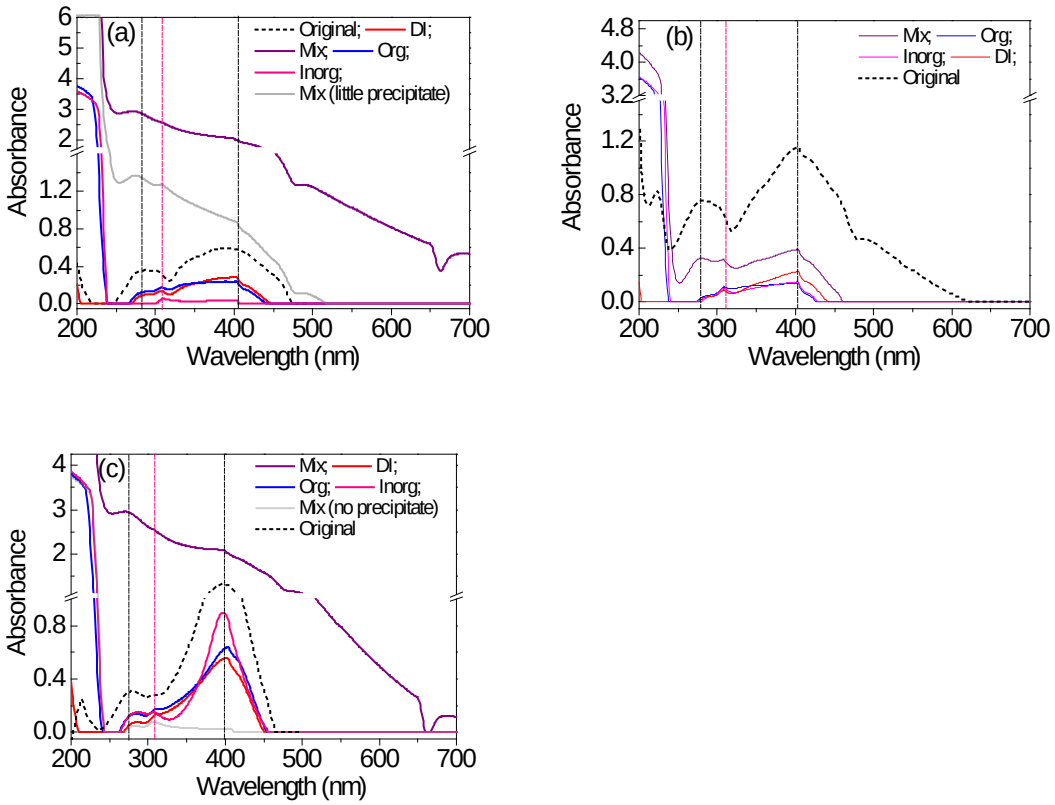


Figure S8. UV-Vis spectra of pristine and reacted AgNP (20 ppm after 7 days) with different surface modifications: (a) Ct, (b) PVP, and (c) GA. (Inorg: inorganic components of synthetic sap; Org: organic components of synthetic sap; Mix: synthetic sap). There are two primary peaks in the UV-Vis spectra of original AgNP, one at 270 nm ($Ag^+$ on the NP surface[12]), and the other at 400 nm (Ag(0) in AgNP[13]). After 7 days in synthetic sap, the main peak at 400 nm was still observed while the peak at 270 nm shifted to 310 nm, which has been associated with the formation of AgCl.[14] Notedly, there was a significant amount of precipitates in Mix sap with SC-AgNP and GA-AgNP dosage after 3 days (also the Mix sap without any NP dosage), but not in PVP-AgNP dosage. While the precipitates are likely due to the "crashing out" of organics in aqueous media with high salinity, PVP might adsorb organics from Mix sap. The precipitates in the Ct-AgNP and GA-AgNP reaction system unfortunately covered the peak of AgNP. However, as we detected residual Ag(0) in both Inorganic and Organic solution with Ct-AgNP or GA-AgNP dosage, it is expected that there were Ag(0) left in synthetic sap after 7 days. While the peak intensity associated with Ag(0) declined after 7 days compared to those of the original AgNP, especially in the Ct-AgNP and PVP-AgNP reaction system, we speculate that the decline of Ag(0) peak intensity was due to the fast aggregation and sedimentation and there was still a considerable amount of Ag(0) in reacted AgNPs in these reaction systems.

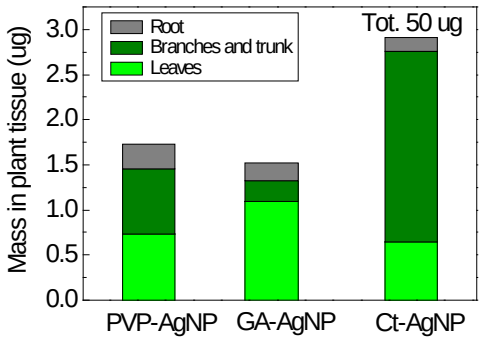


Figure S9. Ag mass recovered in leaves, stem and root from different plants in foliar application with PVP-, GA-, Ct-AgNP after six weeks (Mexican lime, 0.5 ml 100 ppm AgNP exposure). Note, there is no replicate for each type of AgNP

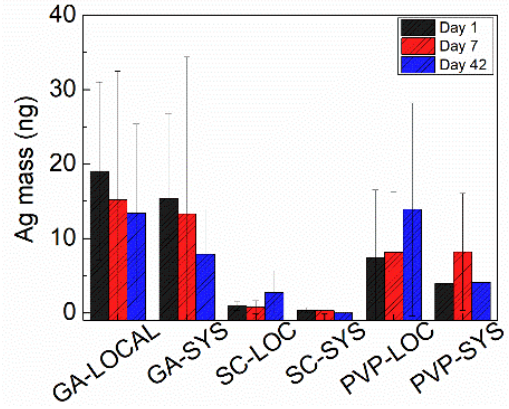


Figure S10. Ag mass in leaf material from trees injected with Ct-AgNPs, PVP-AgNPs, and GA-AgNPs on day 1, 7 and 42 post injection (LOC and SYS: local leaves and systemic leaves).

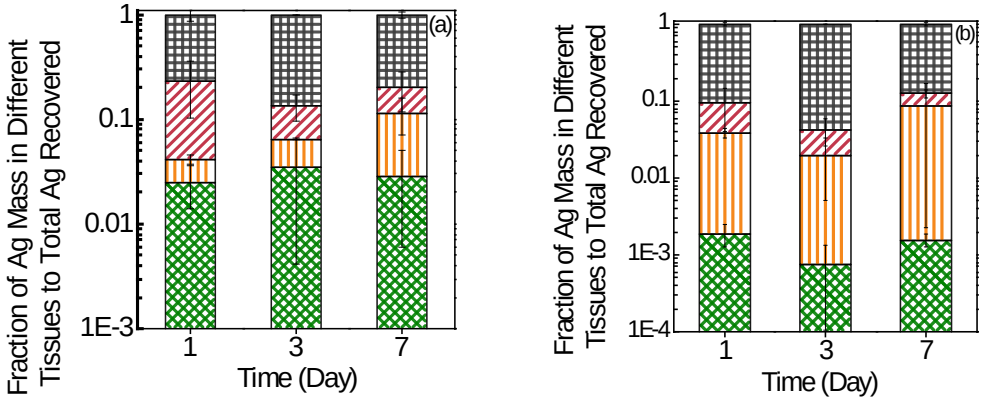


Figure S11. Fraction of Ag mass in dry leaf, branch, trunk, and root to the total Ag mass recovered in trees injected with 10 ppm (a) and 100 ppm (b) GA-AgNPs suspensions (▦, trunk; ▨, root; ▥, branch; ▩, leaf). (2.5-year old clementine mandarin trees, 10 ml AgNPs injection, but injection of 100 ppm GA-AgNPs suspension on Day

3 was not successful and only 7 ml suspension was injected within 2 h). (One-way ANOVA test plus Fisher's LSD test for multiple comparison, $P<0.05$.)

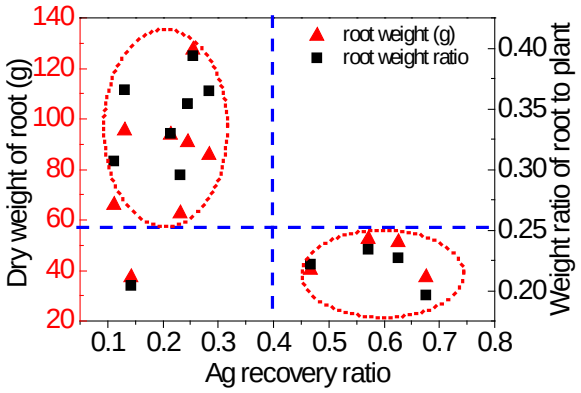


Figure S12. Relationship between Ag mass recovery ratio (Ag mass recovered from all the 2.5-year old clementine mandarin trees to the theoretical value of Ag mass injected) and dry root weight (or the weight ratio of dry root to whole plant).

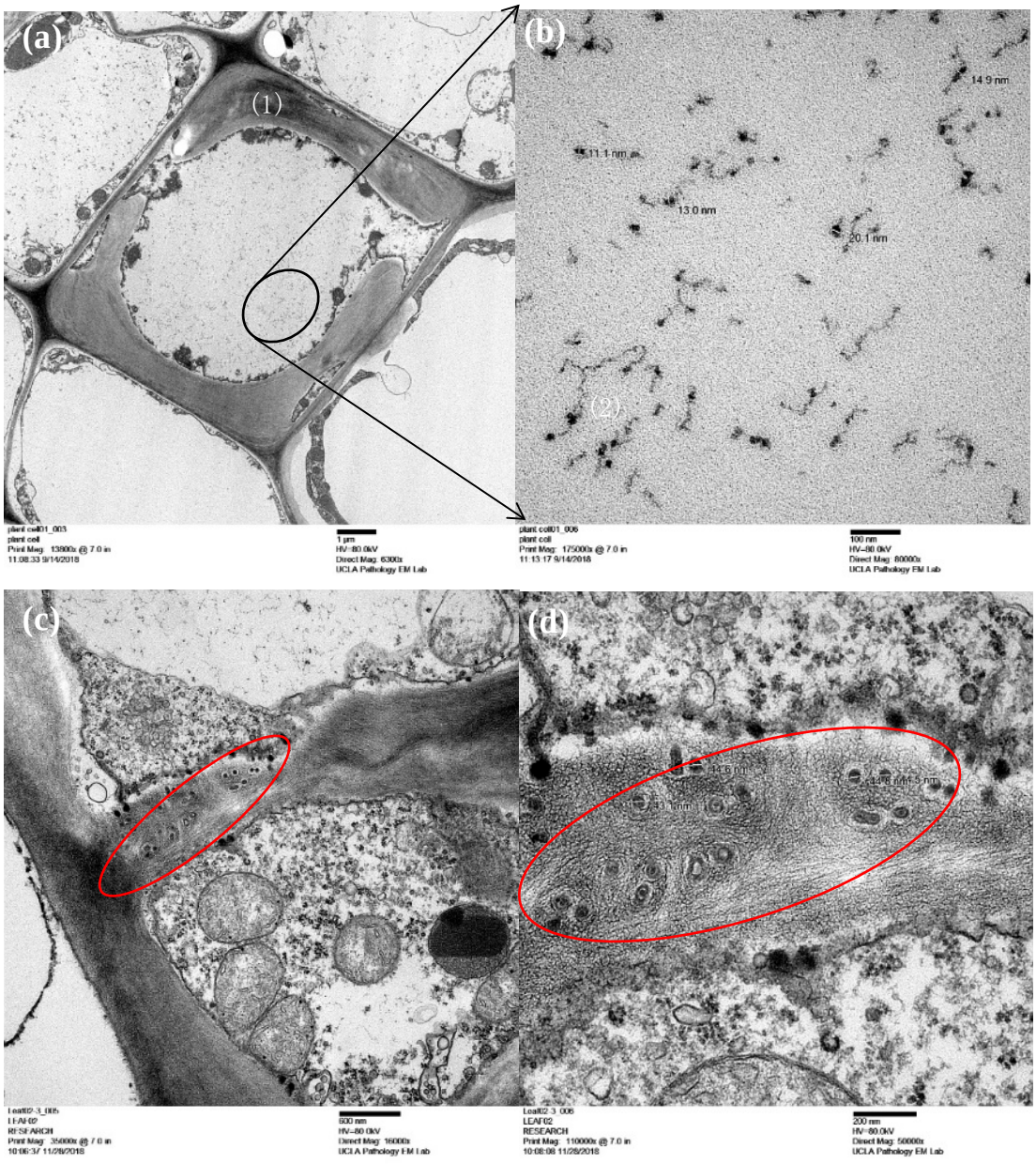


Figure S13. TEM image of cross section of mid-rib (mainly xylem area): (a, b) suspected NPs in xylem (the discontinuous thick wall is helical thickening of a young vessel element; (c, d) suspected AgNPs (in red oval) in membranes or intercellular spaces.

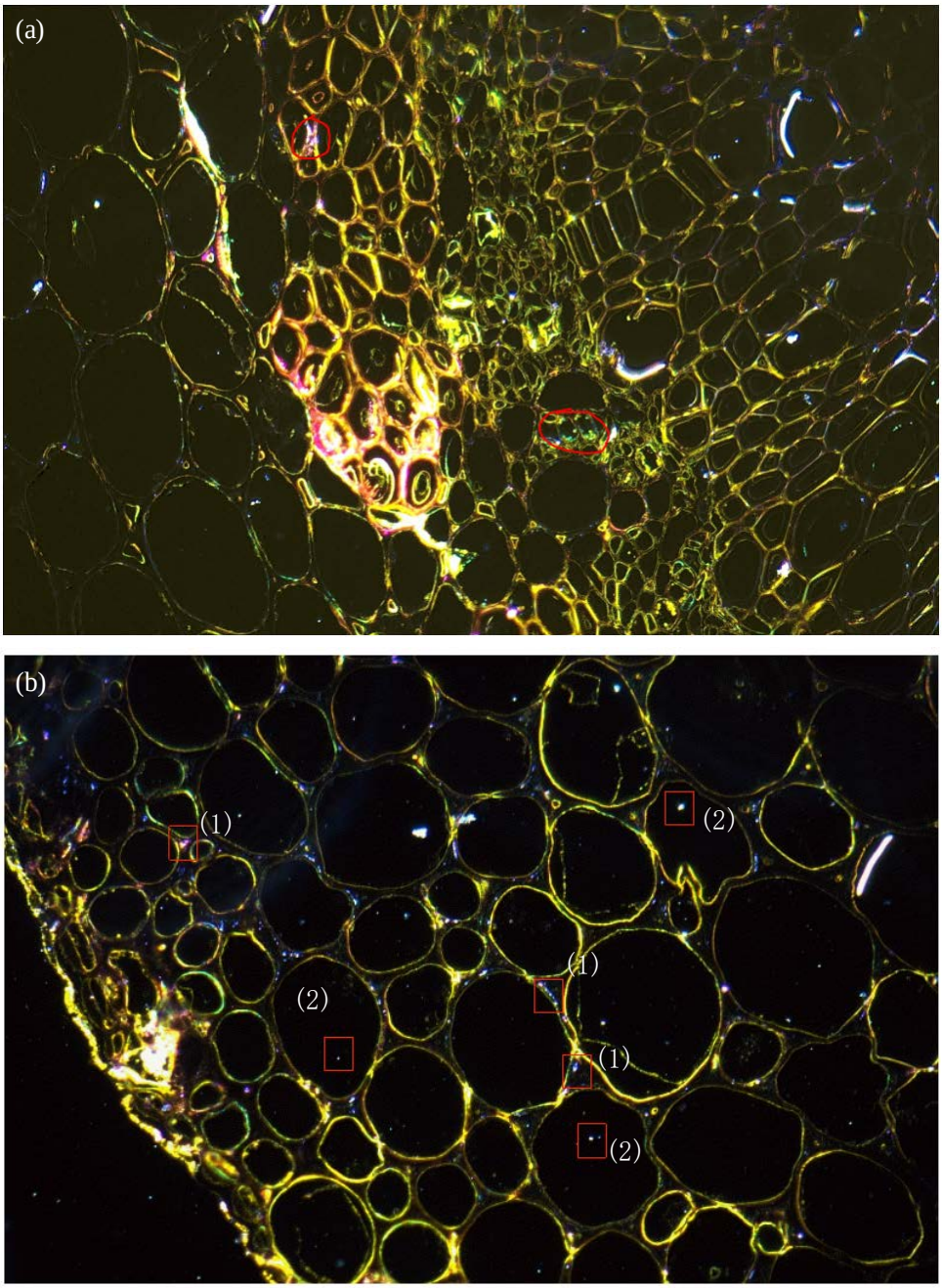


Figure S14. CytoViva analysis on nAg distribution in a microtomed mid-rib of leaf (detected AgNPs shown in circles/rectangles): (a) AgNPs in bundle sheath (1, extracellular) and phloem (2, intracellular), (b) AgNPs in sponge tissue (1, extracellular; 2, intracellular))


Figure S15. (a) Branch feeding and (b) trunk injection for delivering NPs into citrus trees.

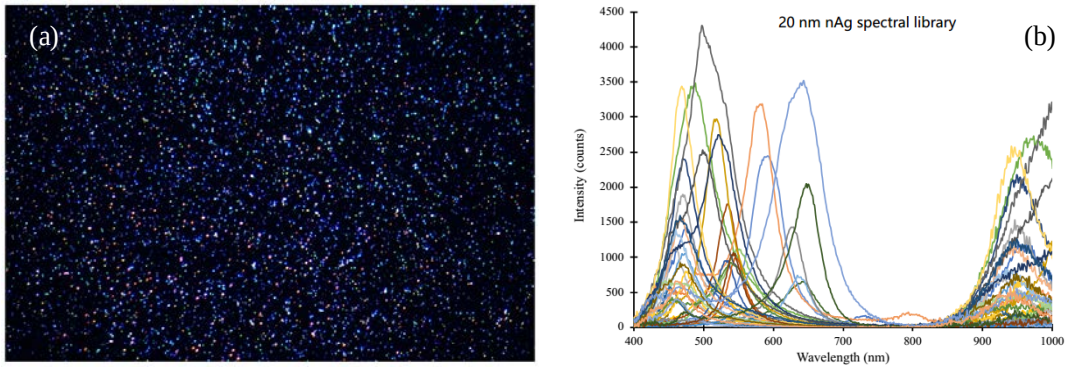


Figure S16. (a) CytoViva analysis of nAg suspension (20 nm) and (b) its spectral library

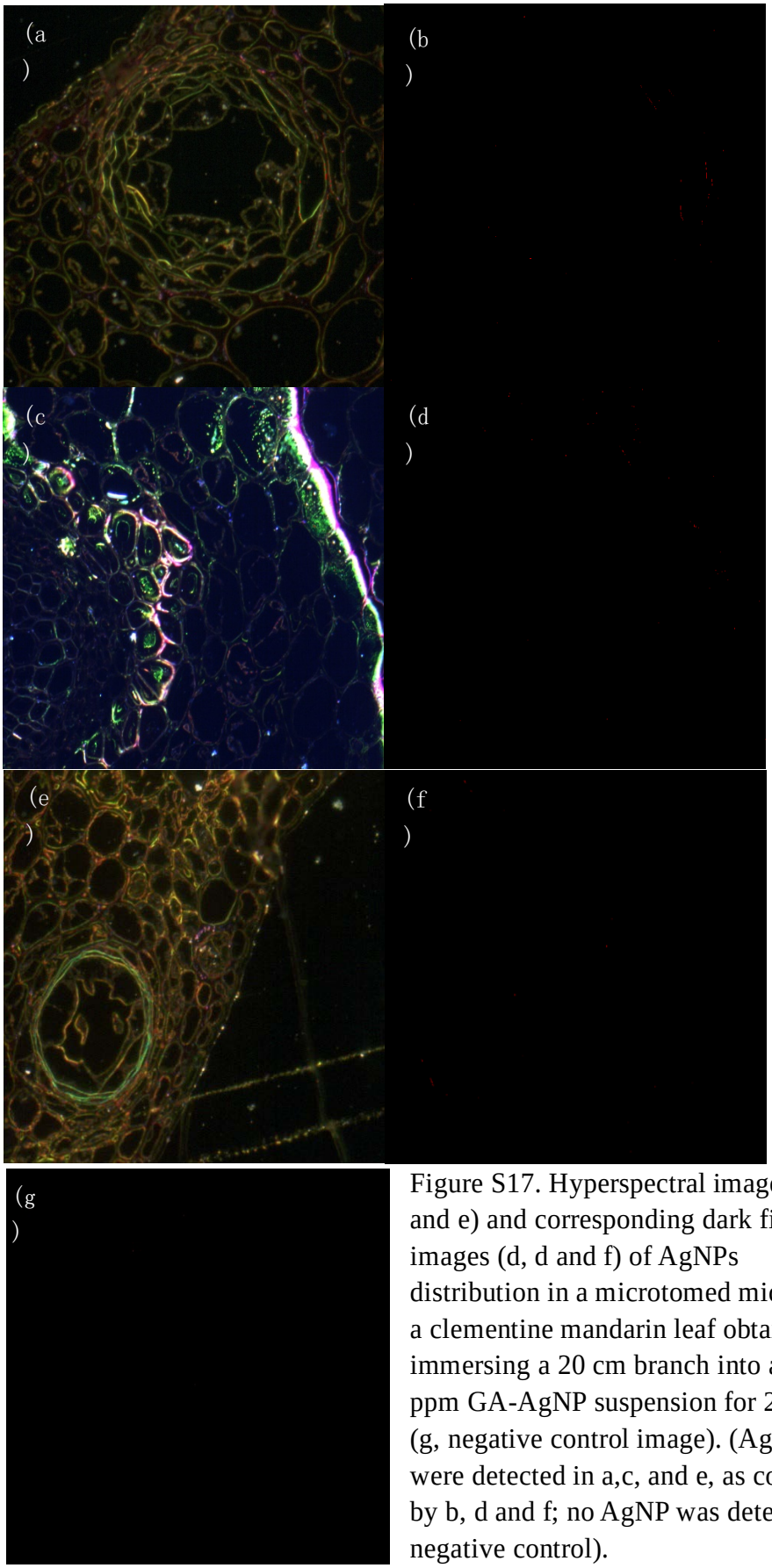


Figure S17. Hyperspectral images (a, c and e) and corresponding dark field images (d, d and f) of AgNPs distribution in a microtomed mid-rib of a clementine mandarin leaf obtained by immersing a 20 cm branch into a 100 ppm GA-AgNP suspension for 24 hours. (g, negative control image). (AgNPs were detected in a,c, and e, as confirmed by b, d and f; no AgNP was detected in negative control).

Table S1. Synthetic sap composition of Mexican lime

| Inorganic solute (mM) | K | Ca | Mg | Na | $NO_3^-$ | $PO_4^{3-}$ | $Cl^-$ |
|---|---|---|---|---|---|---|---|
| | 105 | 90 | 20 | 5 | 5 | 6 | 325 |
| Organic solute (mM) | Malic acid | Proline | Sucrose | Glucose | Fructose | Citric acid | Asparagine |
| | 55.1 | 68.0 | 65.9 | 20.5 | 10.3 | 28.2 | 16.6 |

Note: pH of sap, 5.5 (adjusted with 1 M NaOH and 5% HCl, so actual $Na^+$ and $Cl^-$ concentration in synthetic sap are slightly higher than listed).

**Reference**


(1) Wiesner, M. R.; Bottero, J. *Environmental Nanotechnology: Applications and Impacts of Nanomaterials*; 2nd; McGraw-Hill Education; New York; 2017.

(2) Hahn, M. W.; Abadzic, D.; O'Melia, C. R. Aquasols: On the Role of Secondary Minima. *Environ. Sci. Technol.* **2004**, *38*, 5915–5924.

(3) Shen, C.; Li, B.; Huang, Y.; Jin, Y. Kinetics of Coupled Primary- and Secondary-Minimum Deposition of Colloids under Unfavorable Chemical Conditions. *Environ. Sci. Technol.* **2007**, *41*, 6976–6982.

(4) Salas, W. A.; Ranson, J. K.; Rock, B. N.; Smith, K. T. Temporal and Spatial Variations in Dielectric Constant and Water Status of Dominant Forest Species from New England: Remote Sensing of Environment: Remote Sensing of Forest Ecosystems. *Remote Sens. Environ.* **1994**, *47*, 109–119.

(5) Burke, E. J.; Harlow, R. C.; Ferré, T. P. A. Measuring the Dielectric Permittivity of a Plant Canopy and Its Response to Changes in Plant Water Status: An Application of Impulse Time Domain Transmission. *Plant Soil* **2005**, *268*, 123–133.

(6) Dunlop, J. Membrane Potentials in the Xylem in Roots of Intact Plants. *J. Exp. Bot.* **1982**, *33*, 910–918.

(7) Dunlop, J. The Transport of Potassium to the Xylem Exudate of Ryegrass. *J. Exp. Bot.* **1973**, *24*, 995–1002.

(8) Wright, J. P.; Fisher, D. B. Measurement of the Sieve Tube Membrane Potential. *Plant Physiol.* **1981**, *67*, 845–848.

(9) van Oss, C. J. Hydrophobic, Hydrophilicand Other Interactions in Epitope-Paratope Binding. *Mol. Immunol.* **1995**, *32*, 199–211.

(10) Phenrat, T.; Song, J. E.; Cisneros, C. M.; Schoenfelder, D. P.; Tilton, R. D.; Lowry, G. V. Estimating Attachment of Nano- and Submicrometer-Particles Coated with Organic Macromolecules in Porous Media: Development of an Empirical Model. *Environ. Sci. Technol.* **2010**, *44*, 4531–4538.

(11) Baker, J. A.; Pearson, R. A.; Berg, J. C. Influence of Particle Curvature on Polymer Adsorption Layer Thickness. *Langmuir* **1989**, *5*, 339–342.

(12) Zhang, W.; Qiao, X.; Chen, J.; Wang, H. Preparation of Silver Nanoparticles in Water-in-Oil AOT Reverse Micelles. *J. Colloid Interface Sci.* **2006**, *302*, 370–373.

(13) Karthik, P. S.; Singh, S. P. Conductive Silver Inks and Their Applications in Printed and Flexible Electronics. *RSC Adv.* **2015**, *5*, 77760–77790.

(14) Han, L.; Wang, P.; Zhu, C.; Zhai, Y.; Dong, S. Facile Solvothermal Synthesis of Cube-Like Ag@AgCl: A Highly Efficient Visible Light Photocatalyst. *Nanoscale* **2011**, *3*, 2931.